Effects of post-growth heat treatment on electronic phase diagrams and critical current densities of $Ba(Fe_{1-x}Co_x)_2As_2$ and $BaFe_2(As_{1-x}P_x)_2$ single crystals

S. Ishida,[1,*] D. Kagerbauer,[2] D. Song,[1] H. Ogino,[1] A. Iyo,[1] M. Nakajima,[3] J. Shimoyama,[4] M. Eisterer,[2] and H. Eisaki[1]

[1]*Electronic and Photonics Research Institute, National Institute of Advanced Industrial Science and Technology, Tsukuba 305-8568, Japan*

[2]*Atominstitut, TU Wien, Stadionallee 2, 1020 Vienna, Austria*

[3]*Department of Physics, Osaka University, Toyonaka, Osaka 560-0043, Japan*

[4]*Department of Physics and Mathematics, Aoyama Gakuin University, Sagamihara, Kanagawa 252-5258, Japan*

(Received 16 March 2018; revised manuscript received 13 July 2018; published 20 August 2018)

In this paper, we investigated the effects of annealing on the physical properties of $Ba(Fe_{1-x}Co_x)_2As_2$ and $BaFe_2(As_{1-x}P_x)_2$ single crystals systematically. In both systems, the effects of annealing on the phase transition temperatures and the critical current density J_c are contrasting; the superconducting and magnetostructural transition temperatures T_c and T_{sN}, respectively, increased for all doping levels after annealing, whereas the critical current density J_c only increased around the optimally doped region while it decreased in the other regions. These facts indicate that the changes in T_c and J_c caused by annealing are governed by different mechanisms and that the mechanism for J_c varies depending on the doping level. The results demonstrate that the enhancement of T_c and T_{sN} as well as the decrease of J_c can be attributed to the reduction of disorder, while the enhancement of J_c is associated with the enhanced pinning arising from the antiferromagnetic-orthorhombic phase mixed into the superconducting phase.

DOI: 10.1103/PhysRevB.98.054511

I. INTRODUCTION

Annealing, a heat treatment that causes various effects on materials such as removing defects and dislocations, improving chemical homogeneity or promoting phase separations, introducing or extracting elements from materials, and changing crystal structure or texture, is an essential process to improve material properties. In the field of superconductivity research, annealing has played important roles. For example, the critical current properties of Nb-Ti alloys can be largely enhanced by annealing due to the appearance of the α-Ti phase, leading to the practical applications of superconducting (SC) magnets. For high SC transition temperature (high-T_c) cuprate superconductors, the carrier concentration can be controlled by annealing through the change in oxygen content. Annealing is an essential tool to establish a doping phase diagram and to optimize SC properties of high-T_c cuprates, and thus contributes to the understanding of the mechanism of high-T_c superconductivity as well as the development of superconductivity applications.

Various reports have stated that annealing significantly changes the physical properties of high-T_c iron-based superconductors (IBSs). For example, annealing on as-grown single crystals of *RE*FePO (*RE*, rare-earth elements) [1], $AE(Fe,TM)_2As_2$ (*AE*, alkaline-earth elements; *TM*, transition metals) [2–5], $AEFe_2(As_{1-x}P_x)_2$ [6–8], and $FeTe_{1-x}Se_x$ [9–12] enhances T_c or introduces superconductivity. For a parent $CaFe_2As_2$, which shows a phase transition upon cooling, the annealing condition controls the low-temperature phase, i.e., the antiferromagnetic-orthorhombic (AFO) phase or collapsed-tetragonal (cT) phase [13,14]. In addition, a stacking structure of AFO- and cT-phase layers in a crystal is realized through a proper annealing process. In such a crystal, superconductivity emerges although each layer, either AFO or cT phase, is non-SC [15]. Moreover, the annealing enhances not only T_c but also the critical current density J_c in $FeTe_{1-x}Se_x$ [16,17] and $Ba(Fe_{1-x}Co_x)_2As_2$ [18] single crystals.

For the mechanism of the enhancement of superconducting properties of IBSs by the annealing, various interpretations have been proposed; the annealing (i) improves crystallinity and chemical homogeneity [*RE*FePO, $AE(Fe,TM)_2As_2$, and $FeTe_{1-x}Se_x$] [1–6,9], (ii) removes excess Fe between SC layers ($FeTe_{1-x}Se_x$) [12], (iii) changes the pnictogen height which is correlated with T_c for IBSs [$SrFe_2(As_{1-x}P_x)_2$] [7,8], (iv) leads to interface-induced superconductivity ($CaFe_2As_2$) [15], and (v) promotes clustering of dopant elements which causes nanoscale phase separation into underdoped (UD) or overdoped (OD) regions [$Ba(Fe_{1-x}Co_x)_2As_2$] [18]. Especially for the doped-$AEFe_2As_2$ system, no consensus has been reached regarding the origin of the T_c and/or J_c enhancement caused by annealing. To elucidate the underlying enhancement mechanism, it is desirable to establish experimentally how the effects of annealing on T_c and J_c depend on the dopant elements and concentrations.

In this paper, we systematically investigate the effects of annealing on T_c, the magnetostructural transition temperature T_{sN}, and J_c for $Ba(Fe_{1-x}Co_x)_2As_2$ (Co-Ba122) and $BaFe_2(As_{1-x}P_x)_2$ (P-Ba122) single crystals. After annealing, T_c and T_{sN} were increased at any doping level in both Co-Ba122 and P-Ba122, while J_c was either increased or decreased depending on the doping level. These results indicate the multiple mechanisms and the dominant mechanism changes depending on the doping level. We demonstrate that the effects

*s.ishida@aist.go.jp

of annealing can be consistently understood by considering two factors: the pair-breaking effect of disorder and the vortex pinning arising from the AFO phase.

II. EXPERIMENT

Single crystals of Co-Ba122 and P-Ba122 were grown via the self-flux method using FeAs and Ba_2As_3/Ba_2P_3, respectively [6,19]. The as-grown crystals were sealed in evacuated quartz tubes together with BaAs (for Co-Ba122) or a BaAs/BaP mixture (for P-Ba122) and annealed at 800 °C for two days [6,20–22]. The compositions of the single crystals were determined by performing energy-dispersive x-ray analysis. The samples were cut into rectangular shapes for the physical property measurements. The dependence of the in-plane resistivity $\rho_{ab}(T)$ on the temperature T was measured by employing a standard four-probe method using a physical property measurement system (Quantum Design). The dependence of the magnetization $M(H, T)$ on T and the magnetic field H for the $H//c$ axis were measured using a magnetic property measurement system (Quantum Design). The Bean model was applied to estimate J_c from $M(H)$ [23]. Note that these measurements were performed on the same crystals before and after annealing to ensure accurate evaluation of the annealing effects. In addition, we performed the measurements on several samples at each doping level to confirm the reproducibility.

III. RESULTS

A. Effects of annealing on T_c and T_{sN} for Co-Ba122

First, we analyzed the effects of annealing on T_c and T_{sN} based on $\rho_{ab}(T)$. Figures 1(a)–1(e) show $\rho_{ab}(T)$ for representative Co-Ba122 samples with $x = 0.050$ (UD), 0.057 (slightly UD), 0.061 [optimally doped (OPT)], 0.069 (OPT), and 0.078 (OD). The data for other compositions ($x \geqslant 0.084$) are provided in Fig. S1 in the Supplemental Material [24]. In all of the figures, the black and red points correspond to the as-grown and annealed samples, respectively. Magnified views around T_c are presented in the upper panels. Here we determined T_c based on the zero resistance temperatures. The T_c values are consistent with the onset temperatures of the diamagnetic signals observable in magnetization measurements (see Fig. S2 in the Supplemental Material [24]). After annealing, T_c is increased by 2–3 K for all samples. There is no significant change in the width of the SC transition. The T_c values of each sample before and after annealing (T_c^{AG} and T_c^{Ann}, respectively) are shown in Table S1 in the Supplemental Material [24].

The lower panels show $\rho_{ab}(T)$ below 150 K. The UD samples exhibit increases in ρ_{ab} with decreasing T. This behavior corresponds to the magnetostructural phase transition [25]. For example, for $x = 0.050$ [Fig. 1(a)], the anomalies are evident at 65 and 72 K for the as-grown and annealed samples as indicated by the black and red arrows, respectively. Thus, T_{sN} is increased after annealing. In particular, for $x = 0.061$ [Fig. 1(c)], the anomaly in $\rho_{ab}(T)$ appears after annealing but is not clearly observable for the as-grown sample. Note that the structural and magnetic transition temperatures (T_s and T_N, respectively) are separated for $x = 0.050$, which can be determined based on the T derivative of $\rho_{ab}(T)$. On the other hand, for $x = 0.057$ (as-grown) and $x = 0.061$ (annealed), where the anomaly is very close to T_c, it is difficult to distinguish whether (i) only T_s remains or (ii) T_s and T_N are very close [26]. For more detail, see Fig. S3 in the Supplemental Material [24]. Here, we use T_{sN} for simplicity, which makes it easy to compare the phase diagram before and after annealing.

Figure 1(f) shows the doping phase diagram of Co-Ba122 before and after annealing. For the as-grown samples, the AFO

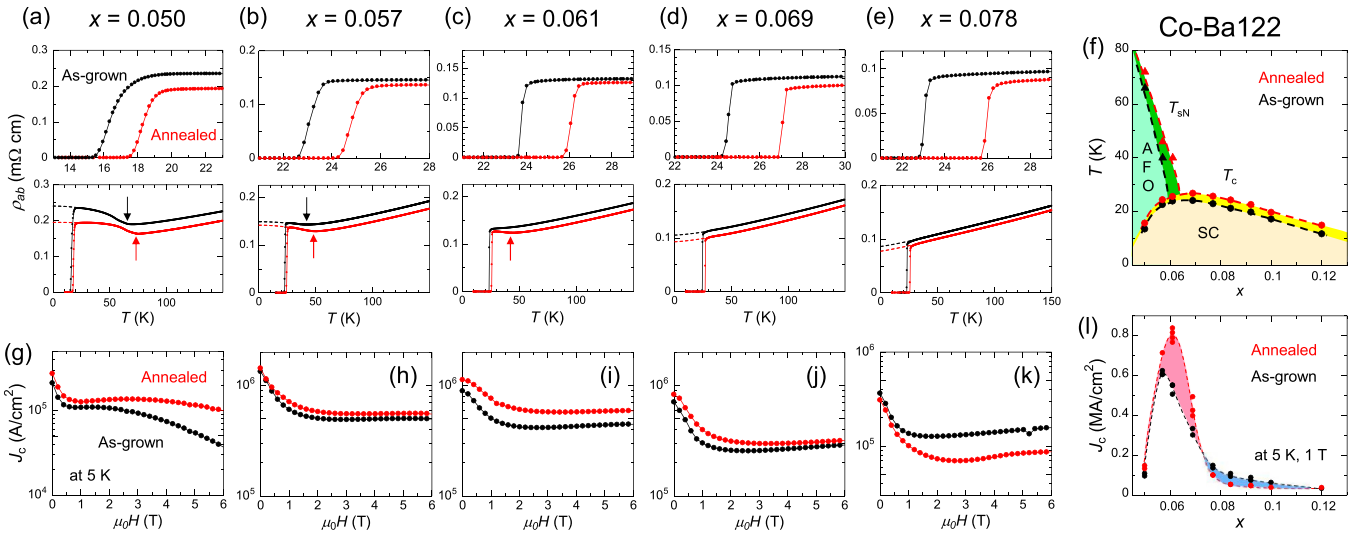

FIG. 1. (a–e) $\rho_{ab}(T)$ for Co-Ba122 samples ($x = 0.050$–0.078). The black (red) data correspond to the as-grown (annealed) samples. The upper panels show enlarged views around T_c. The lower panels depict $\rho_{ab}(T)$ below 150 K. The black (red) arrows indicate T_{sN} for the as-grown (annealed) samples. The dashed lines are the extrapolations to 0 K from the fits to $\rho_{ab}(T)$ using $\rho_{ab}(T) = \rho_0 + AT^{\alpha}$. For the UD samples, $\rho_{ab}(T)$ was fitted using $\alpha = 2$ and $A < 0$. $\rho_{ab}(T)$ of the samples around the AFO end points was not fitted because it is difficult to extract ρ_0 reliably owing to the anomalies just above T_c. (f) Doping phase diagrams before and after annealing. The black (red) circles and triangles indicate T_c and T_{sN} for the as-grown (annealed) samples, respectively. (g–k) H dependence of J_c measured at 5 K. (l) Doping dependence of J_c at 5 K and 1 T.

phase transition line meets the SC phase between $x = 0.057$ and 0.061, while the AFO phase persists to higher doping levels ($x > 0.061$) after annealing. The maximum value of T_c increases from 24.0 to 26.9 K [27]. In addition, T_c reaches its maximum around $x \sim 0.065$ for the as-grown samples, while this position is shifted to $x \sim 0.069$ after annealing.

B. Effects of annealing on J_c for Co-Ba122

Next, we investigated the effects of annealing on J_c. Figures 1(g)–1(k) depict the H dependence of J_c, $J_c(H)$, at 5 K for Co-Ba122 samples with x values corresponding to those in Figs. 1(a)–1(e). There are obvious differences between J_c before and after annealing. In particular, the changes in J_c caused by annealing are distinctly dependent on the doping level. For the samples with $x = 0.050$–0.069, i.e., the UD to OPT samples [Figs. 1(a)–1(d)], J_c is increased after annealing. On the other hand, J_c decreases for the OD sample with $x = 0.078$ [Fig. 1(e)]. The decrease in J_c due to annealing is observable for the samples with x up to 0.10. (Note that J_c increases for these samples at higher T close to T_c owing to the higher T_c after annealing.) For the most OD sample with $x = 0.12$, J_c is increased again after annealing. The results for $x = 0.084$–0.12 are provided in Fig. S1 in the Supplemental Material [24].

Figure 1(l) shows the x dependence of J_c (at 5 K and 1 T), $J_c(x)$, before and after annealing. The multiple data points at each doping level indicate the J_c values measured on different samples with the same x. For the as-grown samples, $J_c(x)$ is characterized by a sharp peak around $x = 0.057$. For the enhanced J_c in the UD region, twin boundaries and magnetic domains arising from the AFO phase are proposed as pinning center candidates [28–30]. Such x dependence is also evident for the annealed samples; specifically, J_c again exhibits a sharp peak. Meanwhile, the increase in J_c due to annealing is the most prominent at $x = 0.061$ close to the OPT region, resulting in a shift of the peak position from $x = 0.057$ to 0.061. Thus, while annealing has the same effect on T_c and T_{sN}, i.e., they always increase, J_c changes differently depending on the doping level.

C. Effects of annealing for P-Ba122

We examined the effects of annealing on the other system, P-Ba122, in a similar fashion. Figure 2 presents $\rho_{ab}(T)$ [Figs. 2(a)–2(e)] and $J_c(H)$ [Figs. 2(g)–2(k)] for the P-Ba122 samples with $x = 0.25$ (UD), 0.29 (slightly UD), 0.30 (OPT), 0.31 (OPT), and 0.38 (OD) before and after annealing (the data for $x = 0.33$, 0.43, 0.52, and 0.61 are provided in Fig. S1 in the Supplemental Material [24]). The obtained doping phase diagrams and $J_c(H)$ are shown in Figs. 2(f) and 2(l), respectively. Comparison of the results for P-Ba122 with those for Co-Ba122 reveals that the effects of annealing on the two systems are similar in that, after annealing, (i) T_c and T_{sN} are increased at any doping level, (ii) J_c is either increased (only for $x = 0.30$–0.31) or decreased depending on the doping level, and (iii) the AFO end point, the maximum position of the SC dome, and the peak position of $J_c(x)$ are shifted toward higher x. Such common effects of annealing on Co-Ba122 and P-Ba122 suggest that the mechanisms underlying the physical property changes are common to the two systems independently of the dopant elements.

IV. DISCUSSION

A. Correlation between changes in T_c and ρ_0

Notably, in addition to the changes in T_c, T_{sN}, and J_c, the residual resistivity ρ_0 is decreased after annealing. It is known that T_c changes with ρ_0 in unconventional superconductors, because of pair breaking caused by disorder. For example, in particle irradiation studies, the change in T_c normalized by T_{c0}—i.e., $\Delta T_c/T_{c0} = (T_{c0}-T_c^{irrad})/T_{c0}$, where T_{c0} and T_c^{irrad} ($T_{c0} > T_c^{irrad}$) are T_c before and after irradiation, respectively—and change in ρ_0 ($\Delta\rho_0 > 0$) are usually compared in discussing the pair-breaking effect. In the present case, considering that the as-grown samples are more disordered, namely, $T_c^{Ann} > T_c^{AG}$ and $\rho_0^{Ann} < \rho_0^{AG}$, we evaluated the change in T_c defined as $\Delta T_c/T_c^{Ann} = (T_c^{Ann}-T_c^{AG})/T_c^{Ann}$ and that in ρ_0 defined as $\Delta\rho_0 = \rho_0^{AG} - \rho_0^{Ann}$.

Figures 3(a) and 3(b) show the x dependences of $\Delta T_c/T_c^{Ann}$ and $\Delta\rho_0$ for Co-Ba22, and Figs. 3(d) and 3(e) show those for

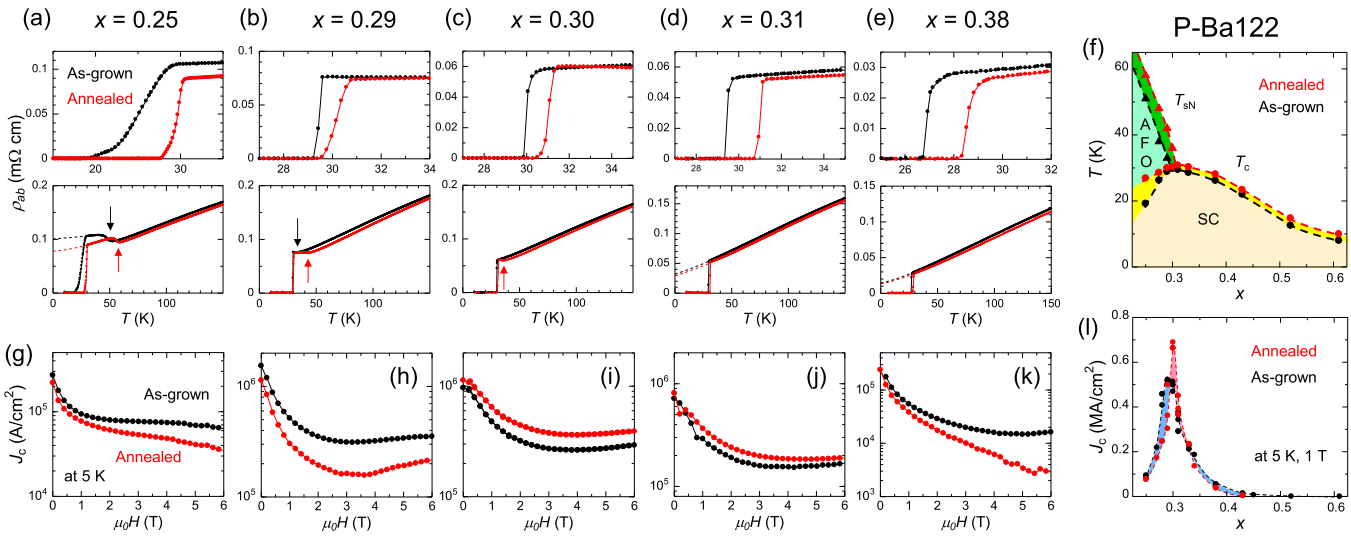

FIG. 2. Same data set as in Fig. 1 for P- Ba122 ($x = 0.25$–0.38). (a–e) $\rho_{ab}(T)$, (f) phase diagrams, (g–k) $J_c(H)$, and (l) $J_c(x)$.

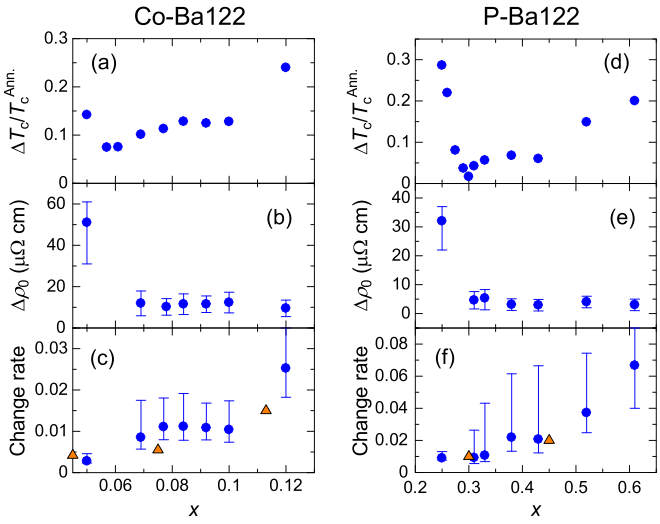

FIG. 3. Doping dependences of (a) $(T_c^{Ann} - T_c^{AG})/T_c^{Ann}$, (b) $\Delta\rho_0$, and (c) change rate of T_c with respect to ρ_0 $\{[(T_c^{Ann} - T_c^{AG})/T_c^{Ann}]/\Delta\rho_0$ (this paper) or $[(T_{c0} - T_c^{irrad})/T_{c0}]/\Delta\rho_0$ (from Ref. [33])$\}$ for Co-Ba122. (d–f) Same data set as in (a)–(c) for P-Ba122, where the $[(T_{c0} - T_c^{irrad})/T_{c0}]/\Delta\rho_0$ data were taken from Ref. [34].

P-Ba122, respectively. The x dependences of $\Delta T_c/T_c^{Ann}$ and $\Delta\rho_0$ are similar for Co-Ba122 and P-Ba122. $\Delta T_c/T_c^{Ann}$ is close to zero around the OPT region, while it is 0.2–0.3 in the UD and OD regions. $\Delta\rho_0$ is large in the UD region and small in the OD region. Based on the data, the change rate of T_c with respect to $\Delta\rho_0[(\Delta T_c/T_c^{Ann})/\Delta\rho_0]$ is plotted in Figs. 3(c) and 3(f) for Co-Ba122 and P-Ba122, respectively. This change rate depends on the doping level; for both Co-Ba122 and P-Ba122, the change rate is small in the UD region and becomes larger as the doping increases.

The quantitative correlation between the changes in T_c and ρ_0 following particle irradiation of IBS has been reported in various studies [31,32]. Here, we compare the present results with the previously obtained change rates of T_c with respect to $\Delta\rho_0$ caused by irradiation, i.e., $(\Delta T_c/T_{c0})/\Delta\rho_0 = [(T_{c0} - T_c^{irrad})/T_{c0}]/\Delta\rho_0$. The triangles in Figs. 3(c) and 3(f) indicate the change rates for Co-Ba122 due to proton irradiation [33] and for P-Ba122 due to electron irradiation [34], respectively. It can be seen that for both Co-Ba122 and P-Ba122 the change rates of T_c due to annealing and particle irradiation, including their doping dependences, exhibit quantitative agreement with each other. Thus, the T_c enhancement caused by annealing can be quantitatively explained by the decrease in ρ_0, i.e., the reduction of disorder. Moreover, it is known from particle irradiation that the introduction of disorder suppresses T_c, while it leads to enhanced pinning and thus enhances J_c. The inverse, a reduction of disorder due to annealing, enhanced T_c, while it weakened pinning due to the disorder, causing J_c to decrease despite the enhanced T_c.

On the other hand, as shown in Figs. 1(l) and 2(l), J_c prominently increases for Co-Ba122 with $x = 0.061$ and P-Ba122 with $x = 0.30$. Note that the increases in T_c for these samples are rather small ($\Delta T_c/T_c^{Ann} \sim 0$) compared with those for other samples [see Figs. 3(a) and 3(d)]. Thus, the large J_c enhancement should arise from significantly enhanced pinning.

B. Correlation between changes in J_c and phase diagram

To determine the origin of the enhanced pinning, we review the changes in $\rho_{ab}(T)$ caused by annealing for Co-Ba122 ($x = 0.061$) and P-Ba122 ($x = 0.30$). In Figs. 1(c) and 2(c), the anomaly in $\rho_{ab}(T)$ corresponding to the magnetostructural phase transition is clearly observable for the annealed samples of both compounds but not for the as-grown samples. This characteristic indicates that the AFO phase is mixed into the SC phase after annealing. Such a correlation between the appearance of the AFO phase and the increase in J_c indicates that the existence of the AFO phase enhances pinning. For these samples, the pinning enhancement due to the AFO phase exceeds the decrease in the contribution from disorder such as crystal defects and strain existing in the as-grown samples, causing J_c to be increased after annealing. Moreover, the AFO phase is considered to compete with the SC phase, possibly resulting in the suppression of T_c [35]. The relatively small increase in T_c can be interpreted as a result of the compensation of two effects: T_c enhancement by the reduction of the disorder and T_c suppression owing to the competition between the AFO and SC phases.

It should be noted that J_c decreases after annealing for the UD P-Ba122 samples ($x = 0.25 - 0.29$), which seemingly contradicts the discussion above. The results suggest that the pinning due to the mixing of SC and AFO phases becomes less effective by underdoping with distance from the AFO end point. One scenario is that the twin domain becomes finer, i.e., the number of pinning centers increases, around the AFO end point, hence J_c is sharply enhanced [28]. Another possibility is that the nature of coexistence of SC and AFO phases changes with doping, resulting in a difference in the pinning strength. In fact, for $Ba(Fe_{1-x}Ni_x)_2As_2$, it was reported that the AF order shows a commensurate-to-incommensurate transition around the end point of the AFO phase [26]. Also, for P-Ba122, it was reported that when the doping approaches the OPT region only part of the sample is magnetically ordered, suggestive of a mesoscopic coexistence of AF and SC phases [36]. Such incommensurate/short-range AF may be a more effective source of pinning than the commensurate/fully-ordered AF phase, and thus J_c largely increases only around the OPT region.

C. Possible origins of unusual pinning

The current results as well as those of our previous studies [29,30,37] strongly suggest the unprecedented pinning mechanism which is related to the presence of the AFO phase next to the SC phase. In our previous papers, we have shown that J_c of the detwinned Co-Ba122 samples shows a large in-plane anisotropy near the AFO-SC phase boundary, where we observe strong enhancement in J_c [37]. Notably, the in-plane anisotropy in J_c, $J_{c,a}/J_{c,b}$, nearly scales with the anisotropy ratio of the normal state in-plane resistivity, ρ_b/ρ_a. The anisotropy of the in-plane resistivity is often attributed as a signature of the electronic nematic order [38,39], which does not break the translational symmetry but breaks the fourfold rotational symmetry of the electronic system. The present results together with our previous ones suggest that the electronic nematicity exists not only in the normal state

but also in the superconducting state and produces unusually strong pinning.

Alternatively, the present observation is consistent with the quantum critical point (QCP) picture. For P-Ba122, it was reported that the vortex core energy shows a significant enhancement around the AFO-SC phase boundary, the QCP in other words [40]. To account for the results, the authors proposed that the energy of the superconducting vortex is enhanced around the QCP, possibly due to the microscopic AF-SC mixing. Because the vortex core energy is related to the pinning strength, enhancement of the vortex core energy leads to the enhanced J_c around QCP, as is observed experimentally in the present case. The enhanced J_c around the QCP was recently also reported for heavy fermion superconductors $CeRh(In, Sn)_5$ [41].

In the high-T_c cuprate superconductors, the signature of the field-induced AF and/or charge density wave orders inside the vortex core has been detected by several experiments, such as neutron scattering [42], scanning tunneling microscopy/spectroscopy [43], nuclear magnetic resonance [44], *etc*., under magnetic fields. The same techniques will be also helpful to reveal the unusual vortex state in the iron-based superconductors.

V. CONCLUSION

In summary, we systematically investigated the effects of annealing on T_c, T_{sN}, and J_c for Co-Ba122 and P-Ba122 and revealed that T_c and T_{sN} increase at any doping level, while J_c increases in a limited doping range around the OPT region and decreases in the other doping regions. We demonstrated that the effects of annealing can be consistently understood for all doping levels by considering two factors: the reduction of disorder and the enhanced pinning due to the AFO phase. The present results also suggest that a proper heat treatment is important for further J_c enhancement of superconducting wires, tapes, and thin films for practical applications.

ACKNOWLEDGMENTS

This work was supported by the Austrian Science Fund (FWF) (Grant No. P22837-N20), the Austria-Japan Bilateral Joint Research Project hosted by the Japan Society for the Promotion of Science (JSPS) and by the Austrian Science Fund (FWF) (Grant No. I2814-N36), and a Grant-in-Aid for Scientific Research (KAKENHI) (JSPS Grants No. JP16K17510 and No. JP16H06439).

[1] R. E. Baumbach, J. J. Hamlin, L. Shu, D. A. Zocco, N. M. Crisosto, and M. B. Maple, New J. Phys. **11**, 025018 (2009).
[2] D. L. Sun, J. Z. Xiao, and C. T. Lin, J. Cryst. Growth **321**, 55 (2011).
[3] S. R. Saha, N. P. Butch, K. Kirshenbaum, and J. Paglione, Physica C **470**, S379 (2010).
[4] K. Gofryk, A. B. Vorontsov, I. Vekhter, A. S. Sefat, T. Imai, E. D. Bauer, J. D. Thompson, and F. Ronning, Phys. Rev. B **83**, 064513 (2011).
[5] G. N. Tam, B. D. Faeth, J. S. Kim, and G. R. Stewart, Phys. Rev. B **88**, 134503 (2013).
[6] M. Nakajima, S. Uchida, K. Kihou, C. H. Lee, A. Iyo, and H. Eisaki, J. Phys. Soc. Jpn. **81**, 104710 (2012).
[7] T. Kobayashi, S. Miyasaka, S. Tajima, T. Nakano, Y. Nozue, N. Chikumoto, H. Nakao, R. Kumai, and Y. Murakami, Phys. Rev. B **87**, 174520 (2013).
[8] T. Kobayashi, S. Miyasaka, S. Tajima, and N. Chikumoto, J. Phys. Soc. Jpn. **83**, 104702 (2014).
[9] T. Taen, Y. Tsuchiya, Y. Nakajima, and T. Tamegai, Phys. Rev. B **80**, 092502 (2009).
[10] T. Noji, T. Suzuki, H. Abe, T. Adachi, M. Kato, and Y. Koike, J. Phys. Soc. Jpn. **79**, 084711 (2010).
[11] Y. Kawasaki, K. Deguchi, S. Demura, T. Watanabe, H. Okazaki, T. Ozaki, T. Yamaguchi, H. Takeya, and Y. Takano, Solid State Commun. **152**, 1135 (2012).
[12] J. Hu, G. C. Wang, B. Qian, and Z. Q. Mao, Supercond. Sci. Technol. **25**, 084011 (2012).
[13] S. Ran, S. L. Bud'ko, D. K. Pratt, A. Kreyssig, M. G. Kim, M. J. Kramer, D. H. Ryan, W. N. Rowan-Weetaluktuk, Y. Furukawa, B. Roy, A. I. Goldman, and P. C. Canfield, Phys. Rev. B **83**, 144517 (2011).
[14] B. Saparov, C. Cantoni, M. Pan, T. C. Hogan, W. Ratcliff II, S. D. Wilson, K. Fritsch, M. Tachibana, B. D. Gaulin, and A. S. Sefat, Sci. Rep. **4**, 4120 (2014).
[15] K. Zhao, B. Lv, L. Deng, S.-Y. Huyan, Y.-Y. Xue, and C.-W. Chu, Proc. Natl. Acad. Sci. USA **113**, 12968 (2016).
[16] Y. Sun, Y. Tsuchiya, T. Yamada, T. Taen, S. Pyon, Z. Shi, and T. Tamegai, J. Phys. Soc. Jpn. **82**, 093705 (2013).
[17] T. Yamada, Y. Sun, S. Pyon, and T. Tamegai, J. Phys. Soc. Jpn. **85**, 024712 (2016).
[18] L. Li, Q. Zheng, Q. Zou, S. Rajput, A. O. Ijaduola, Z. Wu, X. P. Wang, H. B. Cao, S. Somnath, S. Jesse, M. Chi, Z. Gai, D. Parker, and A. S. Sefat, Sci. Rep. **7**, 949 (2017).
[19] M. Nakajima, S. Ishida, K. Kihou, Y. Tomioka, T. Ito, Y. Yoshida, C. H. Lee, H. Kito, A. Iyo, H. Eisaki, K. M. Kojima, and S. Uchida, Phys. Rev. B **81**, 104528 (2010).
[20] S. Ishida, T. Liang, M. Nakajima, K. Kihou, C. H. Lee, A. Iyo, H. Eisaki, T. Kakeshita, T. Kida, M. Hagiwara, Y. Tomioka, T. Ito, and S. Uchida, Phys. Rev. B **84**, 184514 (2011).
[21] S. Ishida, M. Nakajima, T. Liang, K. Kihou, C. H. Lee, A. Iyo, H. Eisaki, T. Kakeshita, Y. Tomioka, T. Ito, and S. Uchida, Phys. Rev. Lett. **110**, 207001 (2013).
[22] S. Ishida, M. Nakajima, T. Liang, K. Kihou, C. H. Lee, A. Iyo, H. Eisaki, T. Kakeshita, Y. Tomioka, T. Ito, and S. Uchida, J. Am. Chem. Soc. **135**, 3158 (2013).
[23] C. P. Bean, Rev. Mod. Phys. **36**, 31 (1964).
[24] See Supplemental Material at http://link.aps.org/supplemental/10.1103/PhysRevB.98.054511 for additional experimental data.
[25] J.-H. Chu, J. G. Analytis, C. Kucharczyk, and I. R. Fisher, Phys. Rev. B **79**, 014506 (2009).
[26] X. Lu, H. Gretarsson, R. Zhang, X. Liu, H. Luo, W. Tian, M. Laver, Z. Yamani, Y.-J. Kim, A. H. Nevidomskyy, Q. Si, and P. Dai, Phys. Rev. Lett. **110**, 257001 (2013).
[27] The maximum T_c value is consistent with the highest T_c reported for the annealed Co-Ba122 single crystals [5].This supports that our samples are well annealed through the present annealing procedure.

[28] R. Prozorov, M. A. Tanatar, N. Ni, A. Kreyssig, S. Nandi, S. L. Bud'ko, A. I. Goldman, and P. C. Canfield, Phys. Rev. B **80**, 174517 (2009).
[29] D. Song, S. Ishida, A. Iyo, M. Nakajima, J.-I. Shimoyama, M. Eisterer, and H. Eisaki, Sci. Rep. **6**, 26671 (2016).
[30] S. Ishida, D. Song, H. Ogino, A. Iyo, H. Eisaki, M. Nakajima, J. Shimoyama, and M. Eisterer, Phys. Rev. B **95**, 014517 (2017).
[31] J. Li, Y. Guo, Z. Yang, K. Yamaura, E. Takayama-Muromachi, H. Wang, and P. Wu, Supercond. Sci. Technol. **29**, 053001 (2016).
[32] M. Eisterer, Supercond. Sci. Technol. **31**, 013001 (2018).
[33] Y. Nakajima, T. Taen, Y. Tsuchiya, T. Tamegai, H. Kitamura, and T. Murakami, Phys. Rev. B **82**, 220504(R) (2010).
[34] Y. Mizukami, M. Konczykowski, K. Matsuura, T. Watashige, S. Kasahara, Y. Matsuda, and T. Shibauchi, J. Phys. Soc. Jpn. **86**, 083706 (2017).
[35] R. M. Fernandes, M. G. Vavilov, and A. V. Chubukov, Phys. Rev. B **85**, 140512(R) (2012).
[36] D. Hu, X. Lu, W. Zhang, H. Luo, S. Li, P. Wang, G. Chen, F. Han, S. R. Banjara, A. Sapkota, A. Kreyssig, A. I. Goldman, Z. Yamani, C. Niedermayer, M. Skoulatos, R. Georgii, T. Keller, P. Wang, W. Yu, and P. Dai, Phys. Rev. Lett. **114**, 157002 (2015).
[37] J. Hecher, S. Ishida, D. Song, H. Ogino, A. Iyo, H. Eisaki, M. Nakajima, D. Kagerbauer, and M. Eisterer, Phys. Rev. B **97**, 014511 (2018).
[38] J.-H. Chu, J. G. Analytis, K. D. Greve, P. L.McMahon, Z. Islam, Y. Yamamoto, and I. R. Fisher, Science **329**, 824 (2010).
[39] I. R. Fisher, L. Degiorgi, and Z. X. Shen, Rep. Prog. Phys. **74**, 124506 (2011).
[40] C. Putzke, P. Walmsley, J. D. Fletcher, L. Malone, D. Vignolles, C. Proust, S. Badoux, P. See, H. E. Beere, D. A. Ritchie, S. Kasahara, Y. Mizukami, T. Shibauchi, Y. Matsuda, and A. Carrington, Nature Commun. **5**, 5679 (2014).
[41] S. G. Jung, S. Seo, S. Lee, E. D. Bauer, H.-O. Lee, and T. Park, Nature Commun. **9**, 434 (2018)
[42] B. Lake, K. Lefmann, N. B. Christensen, G. Aeppli, D. F. McMorrow, H. M. Ronnow, P. Vorderwisch, P. Smeibidl, N. Mangkorntong, T. Sasagawa, M. Nohara, and H. Takagi, Nature Mater. **4**, 658 (2005).
[43] J. E. Hoffman, E. W. Hudson, K. M. Lang, V. Madhavan, H. Eisaki, S. Uchida, and J. C. Davis, Science **295**, 466 (2002).
[44] T. Wu, H. Mayaffre, S. Krämer, M. Horvatić, C. Berthier, P. L. Kuhns, A. P. Reyes, R. Liang, W. N. Hardy, D. A. Bonn, and M.-H. Julien, Nature Commun. **4**, 2113 (2013).